Catalysis Today 147 (2009) 126–132

Contents lists available at ScienceDirect

Catalysis Today

journal homepage: www.elsevier.com/locate/cattod

Electrodeposited Cu–ZnO and Mn–Cu–ZnO nanowire/tube catalysts for higher alcohols from syngas

M. Gupta, J.J. Spivey *

Cain Department of Chemical Engineering, Louisiana State University, Jesse Coates Hall, S. Stadium Drive, Baton Rouge, LA 70803, USA

ARTICLE INFO

Article history:
Available online 23 April 2009

Keywords:
Electrodeposition
Nanowires
Nanotubes
Alcohols
Syngas
CO hydrogenation

ABSTRACT

Cu–ZnO and Mn–Cu–ZnO catalysts have been prepared by electrodeposition and tested for the synthesis of higher alcohols via CO hydrogenation. The catalysts were prepared in the form of nanowires and nanotubes using a nanoporous polycarbonate membrane, which served as a template for the electrodeposition of the precursor metals from an aqueous electrolyte solution. Electrodeposition was carried out using variable amounts of $Zn(NO_3)_2$, $Cu(NO_3)_2$, $Mn(NO_3)_2$ and NH_4NO_3 at different galvanostatic conditions. A fixed bed reactor was used to study the reaction of CO and H_2 to produce alcohols at 270 °C, 10–20 bar, H_2/CO = 2/1, and 10,000–33,000 scc/h g_{cat}. In addition to methane and CO_2, methanol was the main alcohol product. The addition of manganese to the Cu–ZnO catalyst increased the selectivity toward higher alcohols by reducing methane formation; however, CO_2 selectivity remained high. Maximum ethanol selectivity was 5.5%, measured as carbon efficiency.

1. Introduction

The synthesis of higher alcohols from syngas has attracted attention recently as these compounds have been studied for use as neat fuels and fuel additives [1], as well as hydrogen carriers [2,3]. Because syngas can be produced from a wide range of feedstocks such as biomass, coal, and natural gas, the choice of higher alcohols as a potential end product is attractive given the wide range of possible end uses for these oxygenates.

The hydrogenation of CO to produce C_2^+ alcohols has been studied on a number of catalysts, including supported rhodium [4], modified Fischer–Tropsch catalysts [5], sulfides [6], and promoted Cu-based catalysts [7]. Although Rh-based catalysts typically show the greatest selectivity to higher alcohols, the high cost of rhodium may limit its use in large-scale processes. The relatively low cost of Cu-based catalysts, and the fact that they can be modified to increase their selectivity to higher alcohols, suggest that these materials be studied further. Much of the work reported on these catalysts is based on the addition of alkali promoters to methanol synthesis catalysts. However, the hydrogenation of CO to produce higher alcohols is typically limited by low selectivities due to excessive methane and CO_2 formation [2,8].

Catalysts for the synthesis of higher alcohols have most often been prepared by conventional methods such as wet impregnation and co-precipitation. Recently, there has been increased interest in developing novel synthesis approaches such as coating of nanoparticles [9], and the use of shape-selective carbon nanotubes as supports [10].

Here, we report a novel synthesis method to prepare Cu-based catalysts to synthesize alcohols from syngas, based on electrodeposited nanowires and nanotubes of Cu–ZnO and Mn–Cu–ZnO. Electrodeposition is a process in which metals/oxides are deposited on a substrate (cathode) from an aqueous salt solution when an appropriate current/potential is applied. The main advantage of electrodeposition over conventional techniques is the control of the active metal environment, a critical property of a catalyst.

In the present study, two types of catalysts prepared by electrodeposition are compared: Cu–ZnO catalysts representing an unpromoted methanol synthesis catalyst, and Cu–Mn–ZnO, a nominally similar catalyst promoted with Mn. The choice of Mn as a promoter is based on its reported ability to increase selectivity to higher alcohols [7], and the fact that it can be electrochemically co-reduced with Cu in the electrodeposition process used here. Although alkali metals are often used as promoters for Cu-based catalysts [11], their high negative reduction potential, limits the ability to electrodeposit them along with Cu.

To the best of our knowledge, electrodeposited Cu–Zn-based nanowires have not been used as heterogeneous catalysts. However, electrodeposition of ZnO nanowires has been studied for their application in solar cells and sensors [12,13]. Electrodeposited nanowires of Cu_2O have been examined for their photocatalytic properties [13,14], and Cu–Mn–ZnO nanowires have been prepared to enhance the semiconducting properties of

* Corresponding author. Tel.: +1 225 578 3690; fax: +1 225 578 1476.
E-mail address: jjspivey@lsu.edu (J.J. Spivey).

0920-5861/$ – see front matter © 2009 Elsevier B.V. All rights reserved.
doi:10.1016/j.cattod.2009.01.050

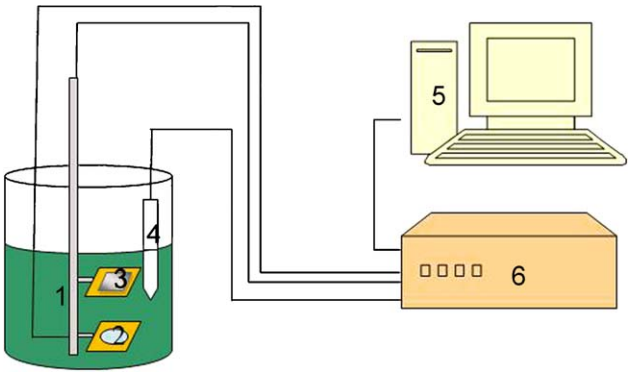

Fig. 1. Electrochemical deposition setup. (1) Electrolyte, (2) cathode (gold sputtered polycarbonate membrane), (3) anode (99.9% pure Zn plate), (4) reference electrode (saturated calomel electrode), (5) computer, and (6) potentiostat.

ZnO [15]. Electrodeposition of nanowires has become an attractive field since the inception of giant magnetoresistance (GMR) [16]. A comprehensive overview of the method and its applications can be found elsewhere [17–19].

2. Experimental

2.1. Electrodeposition

The experimental setup for the electrodeposition of the Cu-based catalysts is shown in Fig. 1. A gold sputtered polycarbonate membrane (Sterlitech®) was used as cathode. The counter electrode was a 99.9% Zn sheet. The reference electrode was an Accumet® saturated calomel electrode (SCE). The electrolytes were aqueous solutions containing varying amount of nitrates of Cu, Zn, Mn, and NH_3. The cell was kept inside a water bath to maintain the required temperature (60 ± 2 °C). Electrolytes were magnetically stirred during experiments to ensure proper mixing of ions and to prevent depletion of ions near the electrode surface. Experiments were performed using an IM-6e potentiostat/galvanostat/impedance spectrometer supplied by BAS Zahner.

The nanowires/tubes were electrochemically deposited by using a template synthesis technique [19] in which an appropriate current/potential is applied to the solution, causing the metals/oxides to deposit within the pores of the gold sputtered membrane (Fig. 2). The pore length and diameter of the membrane were 10 μm and 400 nm, respectively. After deposition, the membrane was dissolved in CH_2Cl_2 and sonicated for 30 min to release the nanowires/tubes.

2.2. Characterization

The bulk elemental analysis was done by a PerkinElmer Optima 3300 DV dual view inductively coupled plasma optical emission spectrometer (ICP/OES). The SEM imaging was done by a model JSM-840A manufactured by JEOL. The XRD analysis was carried out by a Bruker/Siemens D5000 automated powder X-ray diffractometer.

Temperature programmed reduction (TPR) was carried out at atmospheric pressure using an Altamira AMI-200R-HP. First, 10% O_2 in He was passed through the catalyst for 2 h at 400 °C to oxidize any carbon left after dissolution of the polycarbonate membrane. TPR was then carried out in 10% H_2/Ar with a flow rate of 100 scc/min and temperature was ramped from 30 °C to 470 °C at the rate of 10 °C/min.

2.3. Syngas reaction

The fixed bed reaction studies were also carried out in the Altamira AMI-200R-HP. First, 10% O_2 in He was passed through the catalyst for 2 h at 400 °C. Then, the catalyst was reduced using pure H_2 at 320 °C. The reaction was performed at 270 °C, 10–20 bar, and H_2/CO ratio of 2/1. The product stream was analyzed by a 5975x gas chromatography–mass spectrometer (model: G3171A) supplied by Agilent Technologies.

3. Results and discussion

3.1. Electrodeposition

First, appropriate current densities were found using polarization curves. An example of polarization curve is shown in Fig. 3,

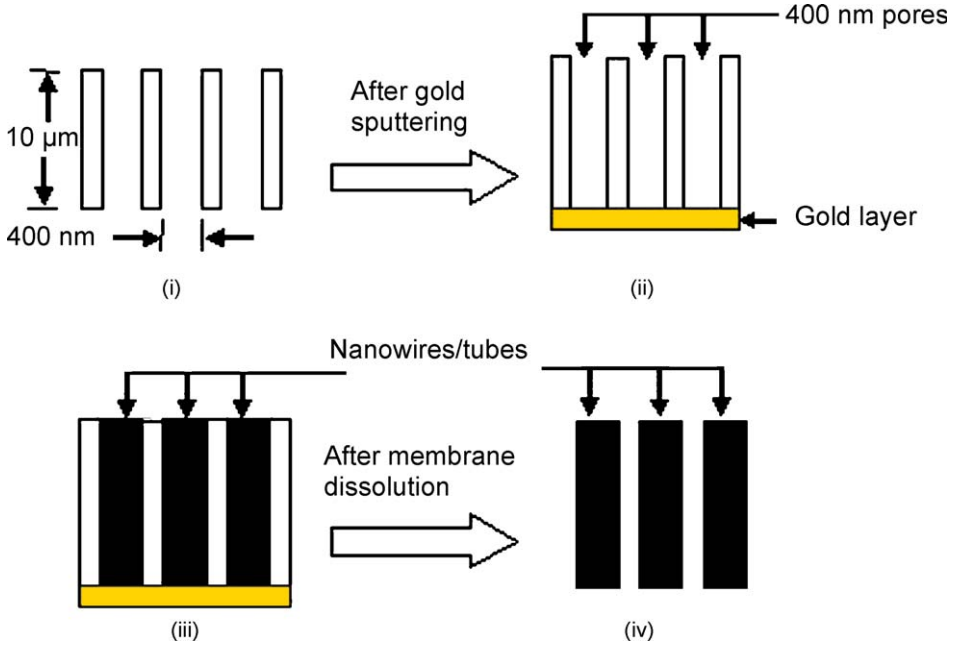

Fig. 2. Schematic for nanowires fabrication (i) cross-sectional view of cylindrical pores in a polycarbonate membrane, (ii) gold sputtered membrane, (iii) filled pores after electrodeposition, and (iv) nanowires after dissolution of membrane in CH_2Cl_2.

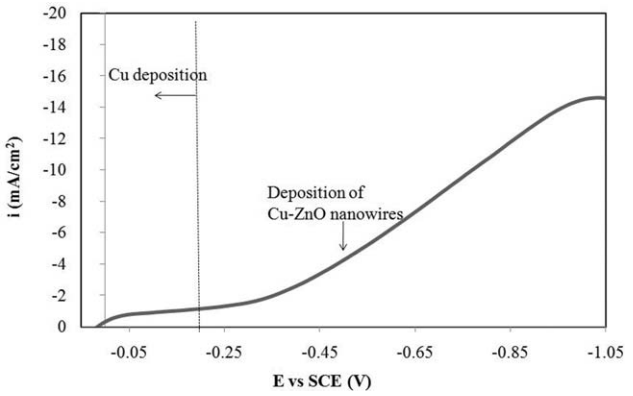

Fig. 3. Polarization curve of electrolyte containing 0.002 M $Cu(NO_3)_2$ and 0.05 M $Zn(NO_3)_2$.

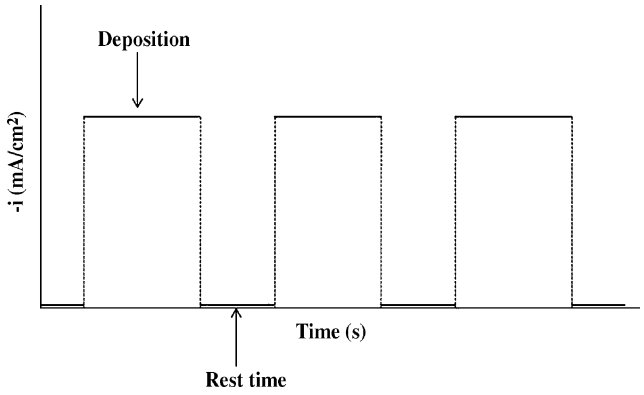

Fig. 4. Pulse scheme for Cu–ZnO nanowires.

representing the effect of potential (V) on current (I) when a potential is applied to the electrode (2) in Fig. 1. Fig. 3 relates a range of total current densities with potential. When the applied potential (V) is low, the current (I) varies linearly with potential. At slightly higher potential, the I–V relationship is exponential (kinetically controlled). When the potential is yet higher, the rate becomes mixed controlled (kinetic and mass transport), and finally at even higher potential the rate of deposition is controlled by mass transfer [20].

In Fig. 3, the left side of the vertical line at about −0.20 V represents a region where there is mostly copper deposition. Copper was deposited according to the following reaction [21], where E^o is the standard reduction potential:

$$Cu^{2+} + 2e^- \rightarrow Cu \quad (E^\circ = +0.10\,V) \tag{1}$$

Copper deposition was found to be mass transfer controlled, since increasing potential from −0.05 V to −0.23 V did not increase the current density significantly.

The sharp increase in the current when potential was more negative than −0.25 V is due to the reduction of nitrate ions as shown in reaction (2). This reaction changed the local pH of the electrolyte from acidic to alkaline:

$$NO_3^- + H_2O + 2e^- \rightarrow NO_2^- + 2OH^- \quad (E^\circ = -0.23\,V) \tag{2}$$

The following reactions show the deposition of other species and standard reduction potential (E°) vs SCE.

Cupric oxide can be deposited according to the following reactions [22]:

$$Cu^{2+} + 2OH^- \rightarrow Cu(OH)_2 \tag{3}$$

$$Cu(OH)_2 \rightarrow CuO + H_2O \tag{4}$$

Cuprous oxide can be deposited according to the following reaction [21]:

$$2Cu(OH)_2 + 2e^- \rightarrow Cu_2O + 2OH^- + H_2O \quad (E^\circ = -0.30\,V) \tag{5}$$

Zinc oxide can be deposited via the following sequence of reactions [23]:

$$NO_3^- + H_2O + 2e^- \rightarrow NO_2^- + 2OH^- \quad (E^\circ = -0.23\,V) \tag{6}$$

$$Zn^{2+} + 2OH^- \rightarrow Zn(OH)_2 \tag{7}$$

$$Zn(OH)_2 \rightarrow ZnO + H_2O \tag{8}$$

3.1.1. Cu–ZnO nanowires

Table 1 shows the effect of electrolyte composition on bulk elemental composition for the two Cu–ZnO catalysts. Increasing copper ions concentration from 0.001 M to 0.002 M at constant zinc concentration increased the copper content in the nanowires.

To change the atomic level interaction of Cu and Zn, a rest time was introduced, as shown in Fig. 4. First, a cathodic current was applied for deposition, followed by a rest time (zero current) to avoid depletion of copper ions, with the goal of obtaining both a uniform composition and higher copper content in the nanowires. Current density, deposition time, and electrolyte concentration were held constant to observe the effect of rest time on copper content in nanowires, as shown in Table 2.

After introducing 20 s and 120 s of rest time during electrodeposition the copper content increased from 28.6% to 42.6% and 42.3%, respectively. The change in rest time from 20 s to 120 s did not affect the Cu content, indicating that 20 s was enough time for copper ions to diffuse to the electrode surface, consistent with theory showing that Cu ions will take 0.1 s to reach the electrode surface from bulk for a 10 μm thick membrane. The time is calculated as follows [24]:

$$t = \frac{l^2}{D} = \frac{(10 \times 10^{-4})^2\,cm^2}{10^{-5}cm^2s^{-1}} = 0.1\,s$$

where, t is the time, l is the distance to be travelled, and D is the diffusion coefficient of the ions.

Fig. 5 is an SEM image of these catalysts, showing that they are in the form of nanowires. The thickness and length of the nanowires were 400 nm and 7 μm, respectively.

3.1.2. Cu–ZnO nanotubes

In addition to nanowires, nanotubes can be produced by electrodeposition. The tube morphology has the advantage of higher surface area, and possibility of shape selectivity which has been shown to increase alcohol selectivity for Rh-based catalysts [10]. Therefore, nanotubes were fabricated using a direct current of

Table 1
Deposition conditions and composition of Cu–ZnO nanowires.

Sample	Electrolyte	Initial pH	Current applied (mA/cm²)	Cu (wt%)	Zn (wt%)
A	0.001 M $Cu(NO_3)_2$ and 0.05 M $Zn(NO_3)_2$	5.0	−5.18	10.1	89.9
B	0.002 M $Cu(NO_3)_2$ and 0.05 M $Zn(NO_3)_2$	4.4	−5.18	28.6	71.4

Table 2
Cu–ZnO nanowires with different rest time (electrolyte: 0.002 M $Cu(NO_3)_2$ and 0.05 M $Zn(NO_3)_2$).

Current density (mA/cm^2)	Deposition time (s)	Rest time (s)	Cu (wt%)	Zn (wt%)
−5.18	7200	0	28.6	71.4
−5.18	20	20 (Short)	42.6	57.4
−5.18	20	120 (Long)	42.3	57.7

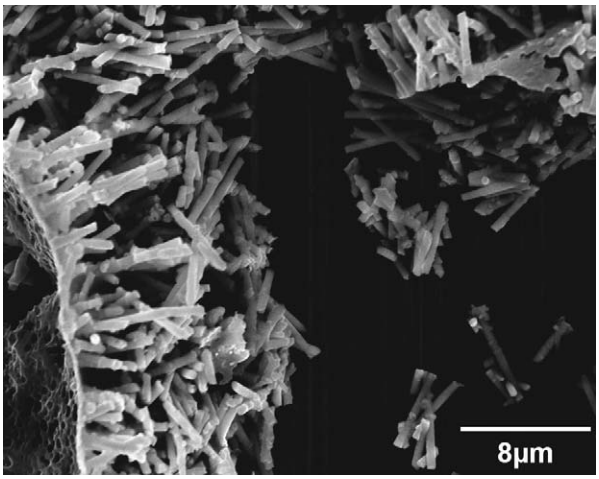

Fig. 5. SEM micrograph of nanowires from electrolyte containing 0.002 M $Cu(NO_3)_2$ and 0.05 M $Zn(NO_3)_2$ and pulse of −5.18 mA/cm^2 for 20 s, 0 for 120 s.

−50.8 mA/cm^2. One of the possible mechanisms for the formation of nanotubes at this high current density is that hydrogen bubbles formation forces the ions to the wall of the membrane (Fig. 6), resulting in no deposition in inner parts of the pores [25]. Fig. 7 shows the nanotubes having inner and outer diameters of 220 ± 20 nm and 400 ± 20 nm, respectively, and containing 2 wt.% Cu and 98 wt.% Zn.

3.1.3. Mn promoted Cu–ZnO nanowires

Table 3 summarizes the synthesis conditions and bulk elemental composition of the Mn-promoted Cu–ZnO nanowires. Manganese is expected to deposit as MnO in the nanowires [26]. Higher current density was used in order to deposit manganese in the nanowires. Due to the increase in current density from −5.18 mA/cm^2 to −25.38 mA/cm^2, Cu content decreased from 28.6 wt.% to 13.5 wt.% and Zn content increased from71.4 wt.% to 82.7 wt.% (Tables 1 and 3). An increase in current density did not increase the deposition rate of Cu since it was mass transport controlled. However, increasing current density increased the deposition rate of ZnO since it was kinetically controlled, resulting

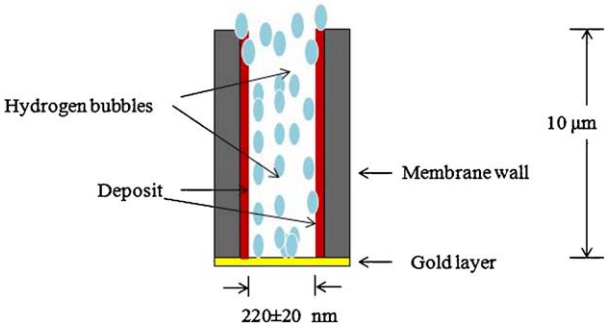

Fig. 6. Generic schematic of nanotube formation.

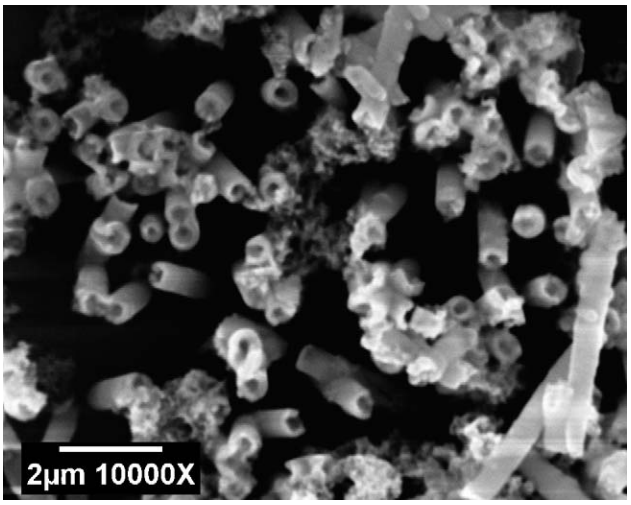

Fig. 7. SEM micrograph of nanotubes from electrolyte containing 0.001 M $Cu(NO_3)_2$, 0.01 M $Zn(NO_3)_2$, and 0.1 M $NH_4(NO_3)_2$.

Table 3
Deposition conditions and composition of Mn–Cu–ZnO nanowires.

Electrolyte	Initial pH	Current applied (mA/cm^2)	Cu (wt%)	Zn (wt%)	Mn (wt%)
0.002 M $Cu(NO_3)_2$, 0.05 M $Zn(NO_3)_2$, 0.05 M $NH_4(NO_3)_2$, 0.02 M Mn $(NO_3)_2$	4.2	−25.38	13.5	82.7	3.8

in less Cu and more Zn in the nanowires. Even though manganese ion concentration in the electrolyte was ten times more than Cu, the nanowires had more Cu (13.8%) than Mn (3.8 wt.%), since Cu is more easily deposited than Mn.

3.2. CO hydrogenation

To study the catalytic properties of the nanowires for syngas conversion, reactions were carried out at varying reaction conditions. Table 4 summarizes the results from different types of nanowire/tube catalysts.

3.2.1. Cu–ZnO nanowires

Fig. 8 shows that an increase in copper content in the nanowires increased the selectivity toward alcohols by reducing the CO_2 formation. Methanol selectivity was more than doubled and ethanol selectivity increased more than 14 times with an increase in copper content. Also, the formation of C_3–C_4 alcohols significantly increased for the nanowires containing more copper. Increasing Cu content from 10.1 wt.% to 28.6 wt.% also increased CO conversion from 0.17% to 0.64%, decreased CO_2 selectivity and increased methane selectivity slightly.

When the rest time was introduced during electrodeposition, total alcohol selectivity decreased, CO_2 selectivity decreased, and methane selectivity increased. (compare Figs. 8 and 9). This difference in their catalytic performance may be due to different compositional uniformity along the length of the nanowires.

Two different rest times of 20 s and 120 s were introduced during electrodeposition. Because the two nanowires prepared using different rest times have the same bulk composition (Table 2), and presumably the same compositional uniformity, the same catalytic behavior might be expected; however, there was a significant increase in higher alcohol selectivity for the

Table 4
Catalytic performance of Cu–ZnO and Mn–Cu–ZnO nanowires/tubes at $H_2/CO = 2/1$, $P = 10$ bar, GHSV = 10,000 scc/h g_{cat}, temperature = 270 °C.

Catalyst wt%			Morphology	Selectivity (%C)[a]					CO conversion
Cu	Zn	Mn		Methanol	Ethanol	C_3–C_4 alcohols	Methane	CO_2	
10.1	89.9	–	Wire	6.5	0.33	ND	49.1	38.9	0.17
28.6	71.4	–	Wire	13.8	4.31	1.1	55.5	19.2	0.64
42.6	57.4	–		6.68	0.68	0.16	64.8	20.7	0.11
	(Short rest time)		Wire						
42.3	57.7	–		6.72	1.86	0.48	65.5	17.5	0.09
	(Long rest time)		Wire						
2	98	–	Tube	15	0.14	ND	67.6	15.4	0.09
13.5	82.7	3.8	Wire	3.8	5.5	10.2	30.7	42.7	0.08

ND: not detected.
[a] Selectively$(\%C) = \frac{NiCi \times 100}{\sum NiCi}$.

where N is the number of carbon atoms in product and C is its concentration (mol%). The products analyzed by GC/MS but not reported here include higher alkanes, *n*-hexane, and propylene. Collectively, these products constitute less than 8%.

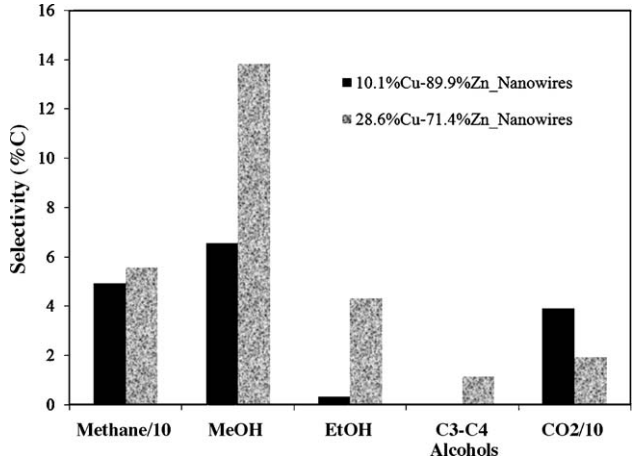

Fig. 8. Selectivities on Cu–ZnO nanowires. Reaction conditions: $H_2/CO = 2/1$, $P = 10$ bar, GHSV = 10,000 scc/h g_{cat}, temperature = 270 °C.

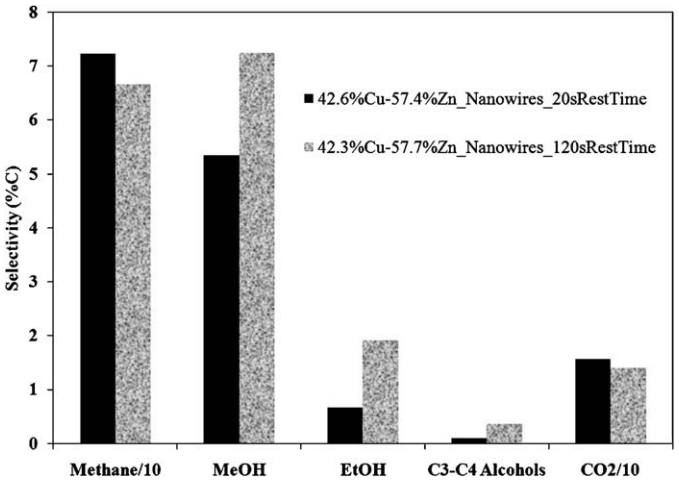

Fig. 10. Selectivities on Cu–ZnO nanowires having different rest times. Reaction conditions: $H_2/CO = 2/1$, $P = 20$ bar, GHSV = 33,000 scc/h g_{cat}, temperature = 270 °C.

nanowires prepared with a 120 s rest time (Fig. 9). Methane and methanol selectivity remained almost same and CO_2 selectivity decreased from 20.7% to 17.5% with the increase in rest time. Increasing the rest time decreased the CO conversion slightly from 0.11 to 0.09%. At other reaction conditions ($H_2/CO = 2/1$, $P = 20$ bar, GHSV = 33,000 scc/h g_{cat}, temperature = 270 °C; Fig. 10), methanol and higher alcohol selectivity increased. However methane and CO_2 selectivity decreased slightly. This may be due to different degree of re-crystallization of the electrode surface and hydrogen release from freshly deposited surface during different rest times [27].

To understand the difference in their catalytic selectivity, the potential transients were analyzed. Fig. 11 shows the potential transients for short and long rest times during electrodeposition. For nanowires having short rest times, the potential did not reach a steady state value after 20 s, indicating that this time was not sufficient for ions to be uniformly redistributed in this diffusion layer [28]. However the potential almost reached a steady state

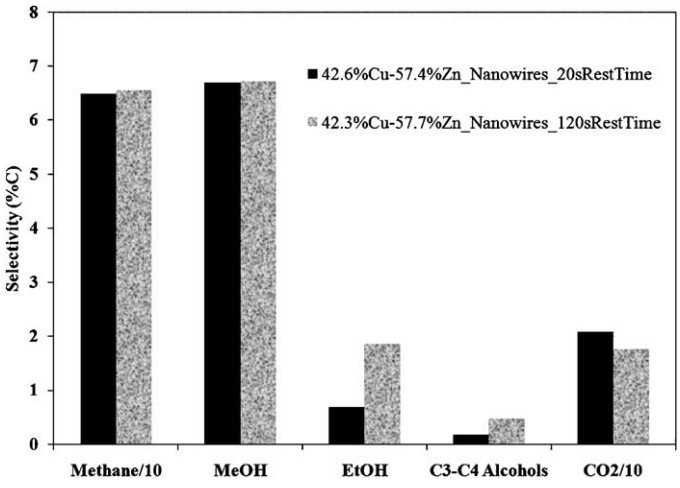

Fig. 9. Selectivities on Cu–ZnO nanowires having different rest times. Reaction conditions: $H_2/CO = 2/1$, $P = 10$ bar, GHSV = 10,000 scc/h g_{cat}, temperature = 270 °C.

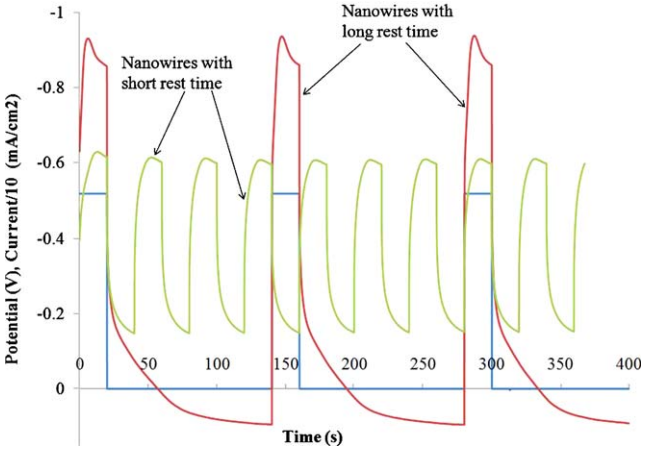

Fig. 11. Potential transients of Cu–ZnO nanowires.

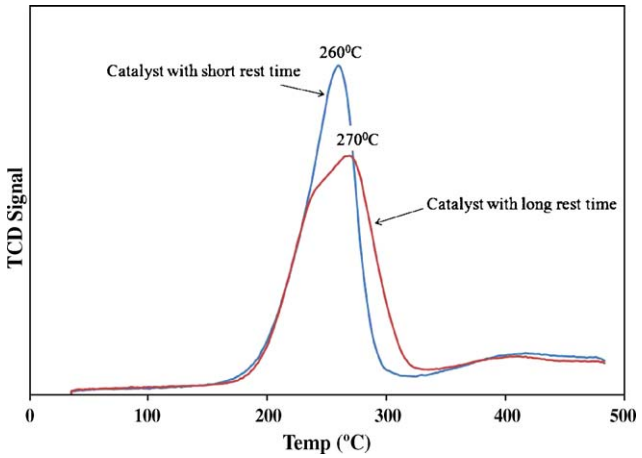

Fig. 12. TPR profile of Cu–ZnO nanowires.

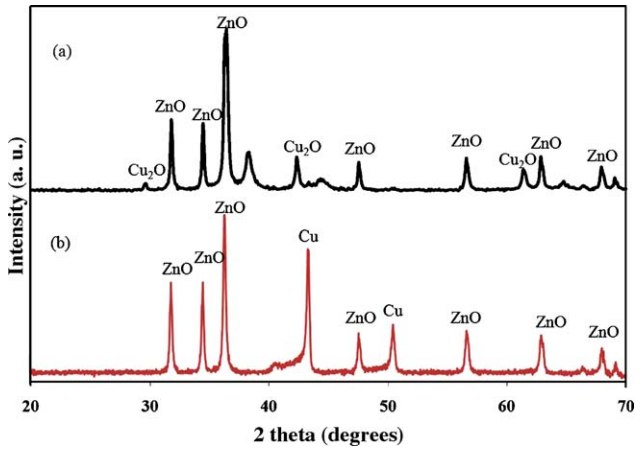

Fig. 13. XRD patterns of Cu–ZnO nanowires: (a) short rest time and (b) long rest time.

value for nanowires that have longer rest time. Rest potentials were different for the two rest times, probably due to different degree of passivation (oxide formation) [27].

To gain insight into the reducibility of the metal oxides in these nanowires, TPR studies were carried out. Fig. 12 shows that both nanowires have lower reduction temperature (260–270 °C) than bulk CuO (400 °C) [29]. This difference in reduction temperature is

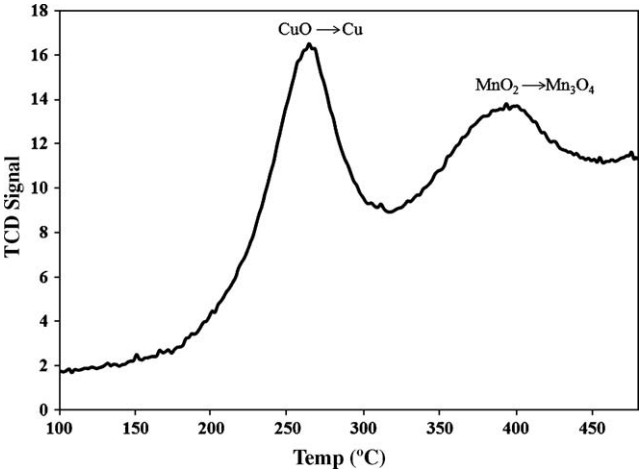

Fig. 14. TPR profile of Mn–Cu–ZnO nanowires.

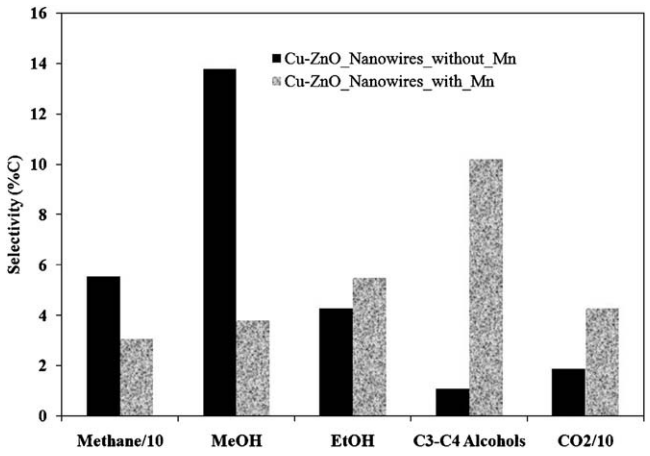

Fig. 15. Selectivities on nanowires with and without manganese. Reaction conditions: $H_2/CO = 2/1$, $P = 10$ bar, GHSV = 10,000 scc/h g_{cat}, temperature = 270 °C.

due to strong interaction between ZnO and CuO observed by other researchers for similar catalysts [30]. The small peak at ≈400 °C is due to residual CuO reduction.

Fig. 12 also shows that increasing the rest time increased the reduction temperature slightly. The reason could be more compact structure of the nanowires having more rest time possibly due to more hydrogen bubble release and also due to different crystalline structure [31]. There is a shoulder between 230 °C and 270 °C for nanowires with long rest time due to the reduction of more dispersed or isolated CuO [32], which appears not to be present in the nanowires prepared with short rest time.

Similarly, XRD analysis (Fig. 13) revealed that different rest times resulted in different crystalline structures. Crystalline ZnO was found in both types of nanowires. However, nanowires with short rest time have crystalline Cu_2O, whereas nanowires with long rest time have crystalline Cu. Crystalline CuO is not found in any of the nanowires, suggesting that any CuO is amorphous.

3.2.2. Cu–ZnO nanotubes

The selectivity of the Cu-Zn nanotubes toward methanol was 15%, which is greater than for the nanowires (Table 4). However, ethanol selectivity was only 0.14% and C_3–C_4 alcohol selectivity was less than the detection limit due to excessive methane formation. The reason could be non-uniform composition due to direct deposition and low copper content. During direct deposition, a constant current was applied without any rest time.

3.2.3. Mn promoted Cu–ZnO nanowires

Fig. 14 shows the TPR results of Mn–Cu–ZnO nanowires. The first peak is due to the reduction of CuO to metallic copper and second peak corresponds to the reduction of MnO_2 to Mn_3O_4 [33].

The addition of manganese increased the selectivity toward ethanol and higher alcohols, consistent with previous studies [7,34] (Fig. 15). This happened due to reduction in methanol and methane formation, however, CO_2 selectivity more than doubled. It is evident from Fig. 15 that the C_3–C_4 alcohols selectivity increased approximately nine times due to the presence of manganese in Cu-ZnO catalyst.

4. Conclusions

Electrodeposited Cu–ZnO nanowires/tubes and Mn–Cu–ZnO nanowires have been successfully prepared using template synthesis method from aqueous electrolytes. For the Cu–ZnO nanowires, deposition and rest times of 20 s and 120 s, respectively, resulted in higher C_2–C_4 alcohols selectivity compared to a

rest time of 20 s. However nanowires without any rest time showed the highest selectivity for higher alcohols.

Although the C_2^+ alcohol selectivity was at most 15.7%, the electrodeposited nanowires may prove to be promising catalysts because of their enhanced selectivity toward higher alcohols at low reaction pressure.

Cu–ZnO nanotubes showed very low selectivity toward alcohols due to excessive methane and CO_2 formation. Therefore, optimization of electrodeposition conditions is required to increase the amount of copper and compositional uniformity and to take advantage of the higher surface area of this morphology.

Addition of manganese to Cu–ZnO nanowires improved the selectivity toward C_2–C_4 alcohols by reducing methane and methanol formation. More research is needed to further enhance the selectivity toward higher alcohols and this can be achieved by optimizing operating variables such as pulse scheme and composition of nanowires.

Acknowledgements

The authors gratefully acknowledge the funding from DOE/NETL (Project # DE-FC26-06NT43024, Project Officer: Dan Driscoll).

References

[1] R.G. Herman, Catal. Today 55 (2000) 233.
[2] J.J. Spivey, A. Egbebi, Chem. Soc. Rev. 36 (2007) 1514.
[3] V. Subramani, C. Song, Catalysis 20 (2007) 65.
[4] M.A. Haider, M.R. Gogate, R.J. Davis, J. Catal. 261 (2009) 9.
[5] K. Takeuchi, T. Matsuzaki, H. Arakawa, Y. Sugi, Appl. Catal. 18 (1985) 325.
[6] D. Li, C. Yang, N. Zhao, H. Qi, W. Li, Y. Sun, B. Zhong, Fuel Process. Technol. 88 (2007) 125.
[7] J.C. Slaa, J.G. Van Ommen, J.R.H. Ross, Catal. Today 15 (1992) 129.
[8] V. Subramani, S.K. Gangwal, Energ Fuels 22 (2008) 814.
[9] N.D. Subramanian, B. Gopalan, V. Palshin, S.S.R.K. Challa, J.J. Spivey, Abstracts of Papers, 236th ACS National Meeting, Philadelphia, PA, United States, August 17–21, 2008.
[10] X. Pan, Z. Fan, W. Chen, Y. Ding, H. Luo, X. Bao, Nat. Mater. 6 (2007) 507.
[11] J. Jorne, C.W. Tobias, J. Appl. Electrochem. 5 (1975) 279.
[12] J. Oh, Y. Jung, J. Lee, Y. Tak, Stud. Surf. Sci. Catal. 146 (2003) 205.
[13] J. Oh, Y. Tak, J. Lee, Electrochem. Solid-State Lett. 8 (2005) C81.
[14] J. Oh, Y. Tak, J. Lee, Electrochem. Solid-State Lett. 7 (2003) C27.
[15] M. Sima, I. Enculescu, M. Sima, M. Enache, E. Vasile, J.-P. Ansermet, Phys. Stat. Solid B: Basic Solid State Phys. 244 (2007) 1522.
[16] T. Osaka, T. Asahi, J. Kawaji, T. Yokoshima, Electrochim. Acta 50 (2005) 4576.
[17] A. Fert, L. Piraux, J. Magn, Magn. Mater. 200 (1999) 338.
[18] C.R. Martin, Science (Washington, D.C.) 266 (1994) 1961.
[19] J.C. Hulteen, C.R. Martin, J. Mater. Chem. 7 (1997) 1075.
[20] M. Paunovic, M. Schlesinger, Fundamentals of Electrochemical Deposition, John Wiley & Sons, Inc., Hoboken, 2006, p. 94.
[21] D.R. Lide, CRC Handbook of Chemistry and Physics, 76th ed., CRC Press, Inc., New York, 1995–96, pp. 8–22.
[22] G.-Q. Yuan, H.-F. Jiang, C. Lin, S.-J. Liao, J. Cryst. Growth 303 (2007) 400.
[23] J.A. Switzer, Am. Ceram. Soc. Bull. 66 (1987) 1521.
[24] E.L. Cussler, Diffusion, Mass Transfer in Fluid Systems, Cambridge University Press, New York, 1997, p. 48.
[25] S.K. Chakarvarti, J. Vetter, J. Micromech. Microeng. 3 (1993) 57.
[26] M. Sima, I. Enculescu, M. Sima, E. Vasile, T. Visan, Surf. Interface Anal. 40 (2008) 561.
[27] D. Landolt, A. Marlot, Surf. Coat. Technol. 169–170 (2003) 8.
[28] U. Cohen, F.B. Koch, R. Sard, J. Electrochem. Soc. 130 (1983) 1987.
[29] M. de los, A. Cangiano, A.C. Carreras, M.W. Ojeda, M. del, C. Ruiz, J. Alloys Compd. 458 (2008) 405.
[30] H.-C. Yang, F.-W. Chang, L.S. Roselin, J. Mol. Catal. A: Chem. 276 (2007) 184.
[31] J. Wu, C.D. Johnson, Y. Jiang, R.S. Gemmen, X. Liu, Electrochim. Acta 54 (2008) 793.
[32] C. Yang, Z. Ma, N. Zhao, W. Wei, T. Hu, Y. Sun, Catal. Today 115 (2006) 222.
[33] K. Ramesh, L. Chen, F. Chen, Y. Liu, Z. Wang, Y.-F. Han, Catal. Today 131 (2008) 477.
[34] C.E. Hofstadt, M. Schneider, O. Bock, K. Kochloefl, Prep. Catal. III 16 (1983) 709.